energies

MDPI

Article

A Diagnosis Method of Bearing and Stator Fault in Motor Using Rotating Sound Based on Deep Learning

Hisahide Nakamura [1,*], Keisuke Asano [2], Seiran Usuda [2] and Yukio Mizuno [2,*]

[1] Research and Development Division, TOENEC Corporation, 1-79, Takiharu-cho, Minami-ku, Nagoya 457-0819, Japan
[2] Department of Electrical and Mechanical Engineering, Nagoya Institute of Technology, Gokiso-cho, Showa-ku, Nagoya 466-8555, Japan; 31413002@stn.nitech.ac.jp (K.A.); 31413029@stn.nitech.ac.jp (S.U.)
* Correspondence: hisahide-nakamura@toenec.co.jp (H.N.); mizuno.yukio@nitech.ac.jp (Y.M.); Tel.: +81-52-619-1707 (H.N.); +81-52-735-5439 (Y.M.)

Abstract: Various industrial fields use motors as key power sources, and their importance is increasing. In motor manufacturing, various tests are conducted for each motor before shipping. The no-load test is one such test, in which, for instance, the current flowing into the motor and temperature of the bearing is measured to confirm whether they are within specific values. Reducing labor, cost, and time in identifying an initially defective product requires a simple and reliable method. This study proposes a new diagnosis to identify the motor conditions based on the rotating sound of the motor in the no-load test. First, the rotating sounds of motors were measured using several healthy motors and motors with faults. Second, their sound characteristics were analyzed, and it was found that the characteristic signals appeared in a specific frequency range periodically. Then, considering these phenomena, a diagnostic method based on deep learning was proposed to judge the faults using long short-term memory (LSTM). Finally, the effectiveness of the proposed method was verified through experiments.

Keywords: diagnosis; bearing fault; short-circuit fault; short-time Fourier-transform (STFT); long short-term memory (LSTM)

Citation: Nakamura, H.; Asano, K.; Usuda, S.; Mizuno, Y. A Diagnosis Method of Bearing and Stator Fault in Motor Using Rotating Sound Based on Deep Learning. *Energies* **2021**, *14*, 1319. https://doi.org/10.3390/en14051319

Academic Editor: Andrea Mariscotti

Received: 27 January 2021
Accepted: 22 February 2021
Published: 1 March 2021

1. Introduction

Various industrial fields use motors as key power sources, and their importance is increasing. According to the failure occurrence rates of the parts in the induction motor, the bearing is the most likely to fail, accounting for up to 41% [1]. Vibration caused by slight holes or scratches in the bearing can affect the product performance. From the standpoint of product management, it is necessary to detect the failure before the shipment of the motor from a manufacturer.

Studies have been conducted to diagnose bearing faults during the past two decades. Most research for detecting bearing faults is based on vibration analysis [2–9]. Motor current signal analysis (MCSA) has also been proposed [10–15], and acoustic emission (AE)-based techniques are receiving increasing attention [16].

In these studies, a rather large hole is introduced to a bearing to simulate the bearing fault. Boudinar et al. [13] conducted experiments using holes with a diameter of 3.0 and 6.0 mm. Leite et al. [12] used the holes with a diameter of 2.3 and 2.8 mm. Saucedo-Dorantes et al. [8] adopted the bearing fault as a hole of 1.191 mm, Hamadache et al. [17] used a hole of 1.0 mm, and Pandarakone et al. [14] used the bearing with holes of 0.5 and 2.0 mm. Among these studies, both [13,14] use FFT. FFT cannot indicate the frequency content of a non-stationary signal change. In [12], fault diagnosis is discussed based on spectral kurtosis and envelope analysis. However, no results or discussion were shown regarding the detection of the smaller size of the hole. The fault-characteristic frequency

pointed out in [17] may be masked by noise because it can be obtained by demodulating the signal.

In addition to bearing faults, various faults occur in the motor. The failure occurrence rates of the stator in the motor account for 37% of faults [1]. The short-circuit fault, which is a major fault in the stator, occurs because of the breakdown of insulation between turns, and ∼80% of all electrical failures in the stator are because of winding insulation failure [18] because of a combination of mechanical, electrical, thermal, and environmental stress. Once a minor short-circuit fault occurs, it can lead to serious failures, such as phase-to-phase short circuit fault and ground fault, which may result in industry shut-down.

Regarding the short-circuit fault, several diagnostic methods have been proposed [19–23]. Yang [19] proposed a detection method using the voltage difference between two neural points. Bouzid et al. [20] proposed a fault diagnostic system based on an artificial neural network to detect several inter-turn short-circuit faults and phase-to-phase faults. Pandarakone et al. [21] proposed a method for discriminating between a healthy and a one-turn short-circuit fault by distortion ratio. Saleh et al. [22] presented an analysis and development of a new method for electric fault detection in induction motor drives based on extracting the magnitudes and phases of high-frequency sub-band contents in stator currents. Irhoumah et al. [23] presented a statistical methodology for detecting inter-turn short-circuit faults using a correlation coefficient obtained from an external magnetic field measured in the machine vicinity. As for deterioration, fundamental experiments are performed [24,25].

Motor manufacturers conduct various tests on each motor before shipping, of which the no-load test is one. In the no-load test, the current flowing into the motor and temperature of the bearing are measured at a given rotating speed. To reduce labor, cost, and time in identifying an initially defective product, a simple and reliable test method requires. It is desirable to detect a small-size hole and identify the faults. Therefore, further experiments using a bearing with a small-size hole are necessary. A discussion of a proper diagnostic method is also needed to implement the identification of the faults. Moreover, if multiple evaluations can be made in one test, the required time for the test of the motor will be shortened. As a result, productivity will be improved. Although many diagnosis methods have been proposed, there seem no studies that diagnose the several kinds of bearing faults and the short-circuit fault in the same framework simultaneously.

This study proposes a novel diagnostic method that enables to identify the several faults based on the rotating sound of the motor during a no-load test, which satisfies the requirements described above. In Section 2, experiments are performed. Several motors with slight faults are prepared, and the rotating sounds of motors are measured. In Section 3, sounds measured in Section 2 are analyzed using a short-time Fourier-transform (STFT), and time and frequency characteristics of the level of rotating sounds are discussed. In Section 4, a methodology is explained. Here, a diagnostic method is proposed to identify the motor condition based on deep learning using long short-term memory (LSTM). In Section 5, the effectiveness of the proposed method is verified through some experiments. The article ends with a constructive conclusion of obtained results.

2. Experiments

2.1. Experimental Setup

The flowchart of this experiment is shown in Figure 1. Motors with several failure conditions as well as healthy motors were running under no-load conditions, and rotating sounds were measured. After then, these sounds were analyzed in the next section.

Figure 2 shows the experimental setup. A three-phase induction motor (2.2 kW, 200 V, 8.5 A, 1740 min^{-1}) was used as a specimen. The commercial power source AC200V was used as the power source of the motor. The structure of the stator winding was a double−star connection. The rotating sounds of motors were measured using a microphone (Sanwa Supply, CMS−V40BK) that was set near the front of the end bracket of the motor,

and the rotating sounds were measured for a few minutes under no-load condition. The sampling frequency of the microphone was 44.1 kHz.

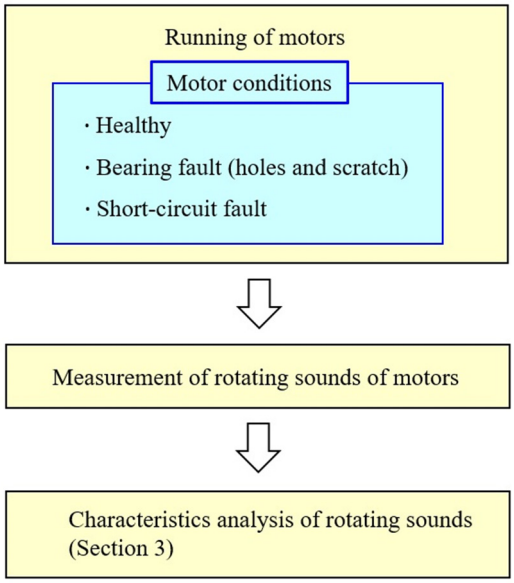

Figure 1. Flowchart of experiments.

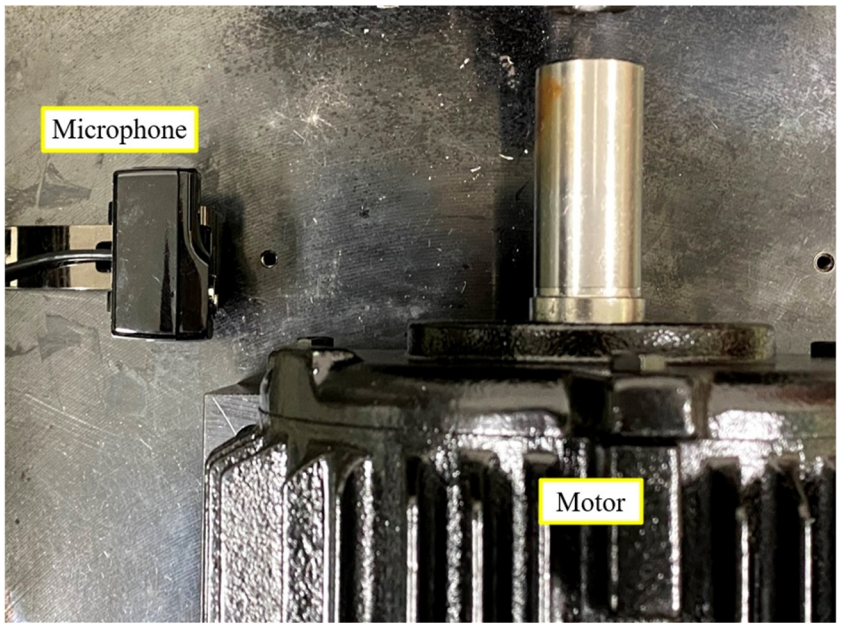

Figure 2. Experimental setup.

2.2. Reproduction of Faults

It is tedious and expensive to collect motors with damage in the bearing, which occurred during the operation at the site. In this study, three types of artificial faults were introduced to the outer raceway of the motor's bearing. The types of faults were one hole with a diameter of 0.5 mm, one hole with a diameter of 2.0 mm, and two holes with a diameter of 2.0 mm. In the case of the two holes, their holes were, respectively, disposed of in positions displaced 180° from each other. Figure 3 shows photographs of these faults.

If a scratch appearing on the bearing was undetected at an early stage, it could increase in size as the motor runs. To simulate this and allow the progression of a fault on the outer raceway of the bearing to be analyzed, a 10 mm scratch was induced (Figure 4).

The short-circuit fault was also artificially induced in this study. The short-circuit faults were made by removing the enamel insulation at the first and second coil in the winding and connecting them with solder. Figure 5 shows the one-turn short-circuit fault.

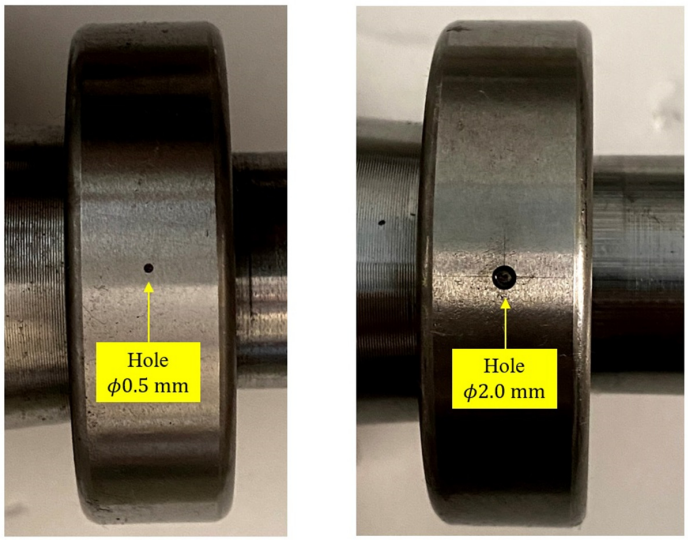

Figure 3. Bearing faults. (**a**) A hole of 0.5 mm, (**b**) a hole of 2.0 mm.

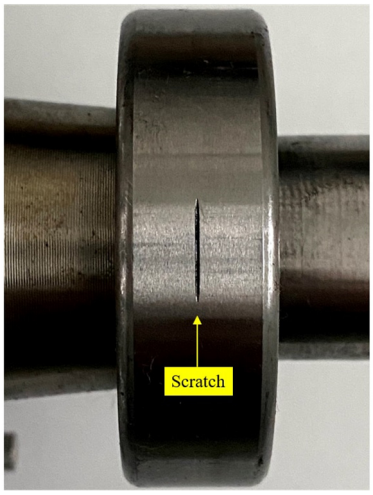

Figure 4. Scratch fault.

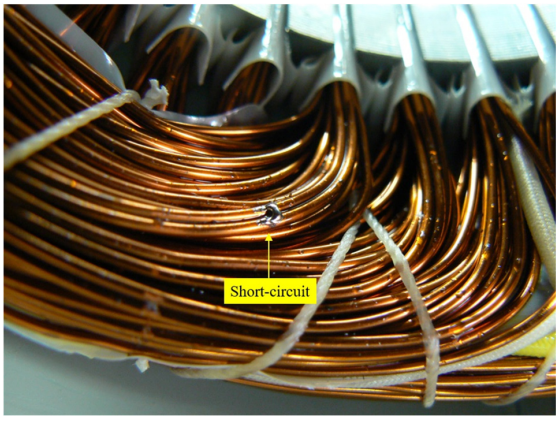

Figure 5. One-turn short-circuit fault.

3. Characteristics of Rotating Sounds of Motors under Each Condition

3.1. Experimental Results

Figure 6 shows example spectra of rotating sound obtained for five healthy motors. A good similarity of the sound spectrum was confirmed between healthy motors. Typical sound spectra of 5 kinds of faulty motors are shown in Figure 7. The sound spectrum of a healthy motor is also shown in the figure for reference. It was clear that the sound spectrum was affected by a fault.

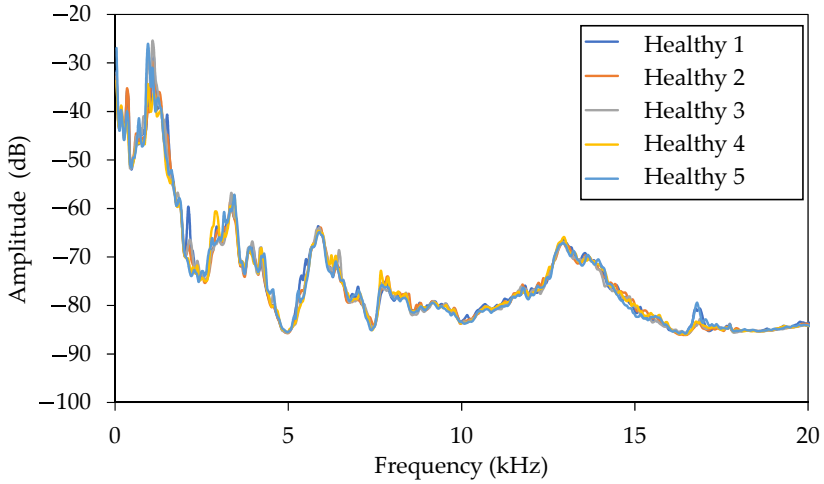

Figure 6. Spectra of the rotating sound of five healthy motors.

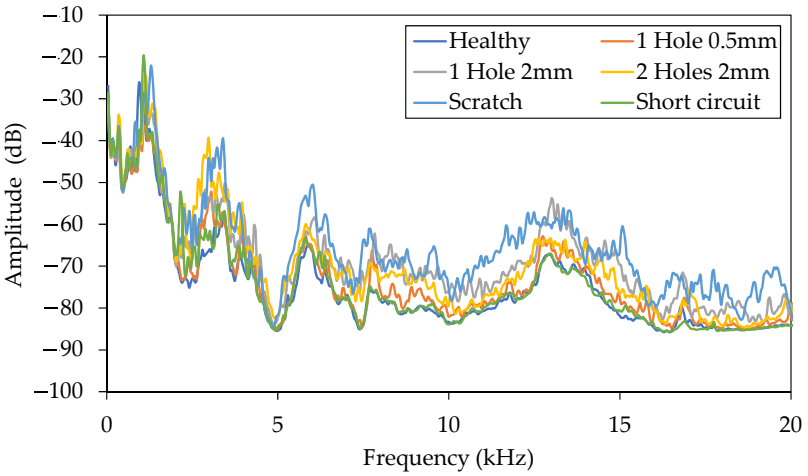

Figure 7. Spectra of the rotating sound of faulty motors.

3.2. Analysis of Spectrum of Rotating Sound Based on Short-Time Fourier-Transform (STFT)

When the motor runs at a constant speed, it is expected that a periodic signal will be observed in its rotating sound. For this reason, the sound spectrum time–frequency analysis was performed for the originally recorded rotating sounds of the motors. The sound data were subdivided into tens of 1 s sound data sets, and STFT was applied for them. STFT had an advantage because it represents the relationship between the time and frequency of the signal. The Hamming window was used as a window function in the STFT, and 128–points FFT was performed by shifting the overlapping time by 0.59 ms.

Figures 8–12 show the spectrum results for each fault. Though hundreds of STFT spectra were obtained by the experiments, representative spectra for each bearing condition are displayed in these figures. They represent the relationship between time (ms), frequency (Hz), and sound pressure (dBA). In case of a healthy condition, two new motors were

prepared, and the rotating sounds were measured to confirm the individual difference in the sound spectrum. Consequently, the two spectra were similar.

In the case of the hole in the bearing, a periodic signal was observed near the 3 kHz band. In particular, a periodic signal at about 4 ms intervals could be observed. Furthermore, the larger the hole size and the more the number of hole, the louder the periodic signals by comparing Figures 9–11.

The fundamental acoustic experiments were performed to declare the generation mechanism of the impact sound generated from plates subjected to colliding spherical bodies [26], which clarifies the effect of geometric and material properties of the plated and spherical bodies on a frequency spectrogram of sound pressure. According to work, the principal frequency components, including the impact sound generated from the steel plate subjected to the collision of the steel spherical bodies, were approximately 500 Hz, 1.5, and 3 kHz. The appearance of the frequency component (3 kHz) observed in the present experiments matched past fundamental experiments.

In the case of the scratch, the whole spectrum was similar to the spectrum of the hole with a diameter of 2.0 mm, compared to Figures 10 and 12. However, the spectrum around 3 kHz seemed to be large and expands slightly in the time axis because the time for a ball in the bearing to pass beneath the scratch on the outer raceway was longer than that of the one hole.

In the case of the short-circuit fault, a strong sound was observed between 500 Hz and 1.5 kHz (Figure 13). This motor runs 30 rotations per second. By displaying the spectrum for 100 ms, as shown in Figure 14, the periodic spectrum was observed at a 33 ms interval between 500 Hz and 1.5 kHz and near 3 kHz, respectively, because of the appearance of the deviation of the magnetic field caused by the short-circuit fault. Thus, spectra obtained by STFT had a plethora of information depending on the motor conditions, and we used these results in the next diagnostic step.

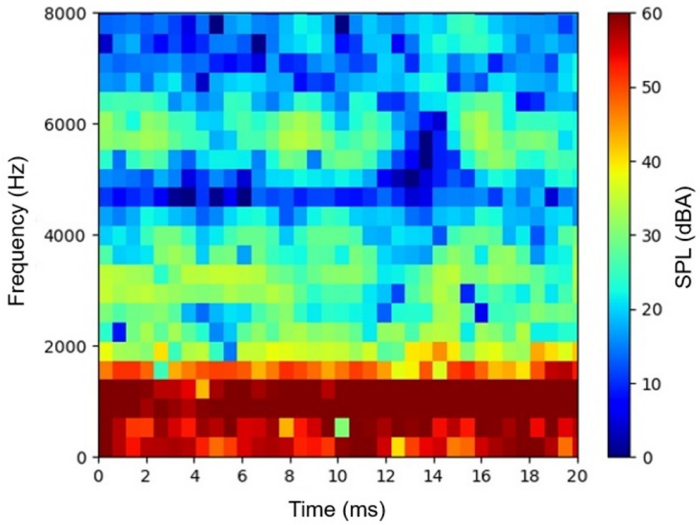

Figure 8. Spectrum for the healthy motor.

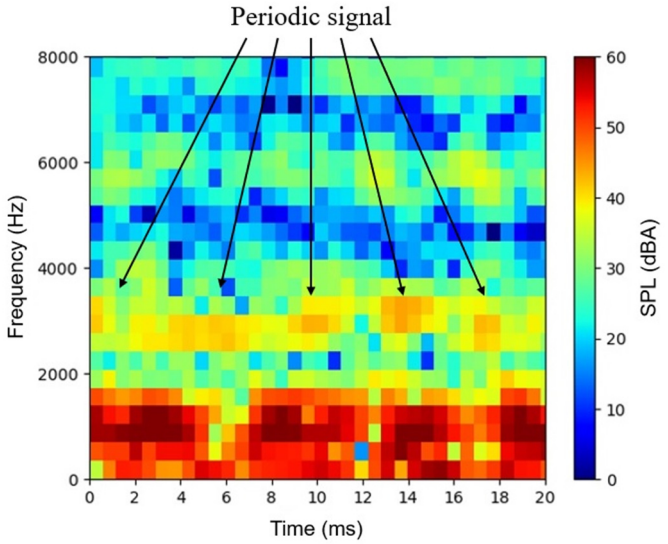

Figure 9. Spectrum for the motor with one hole with a diameter of 0.5 mm.

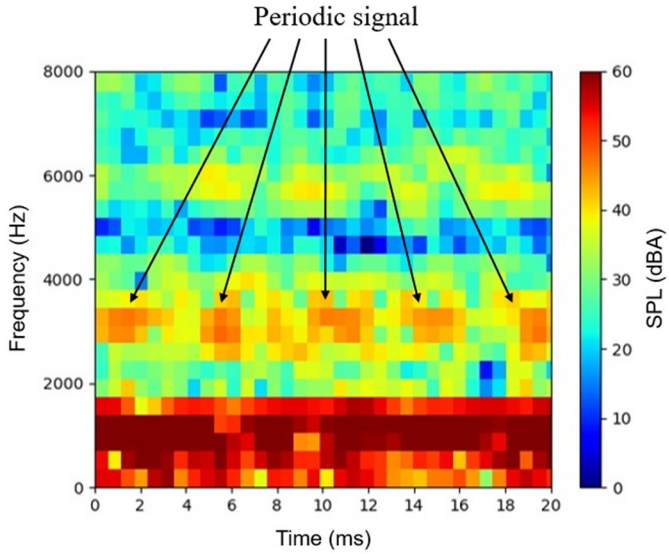

Figure 10. Spectrum for the motor with one hole with a diameter of 2.0 mm.

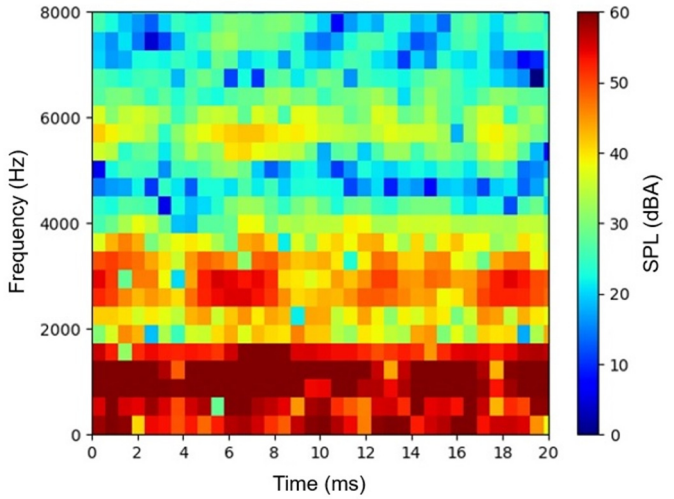

Figure 11. Spectrum for the motor with two holes with a diameter of 2.0 mm.

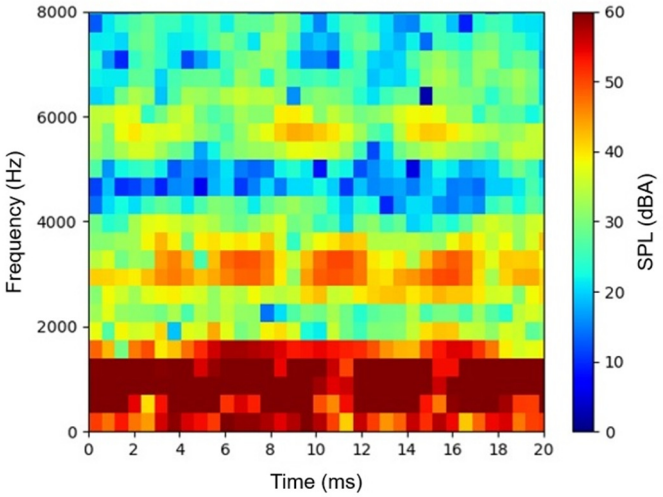

Figure 12. Spectrum for the motor with a scratch.

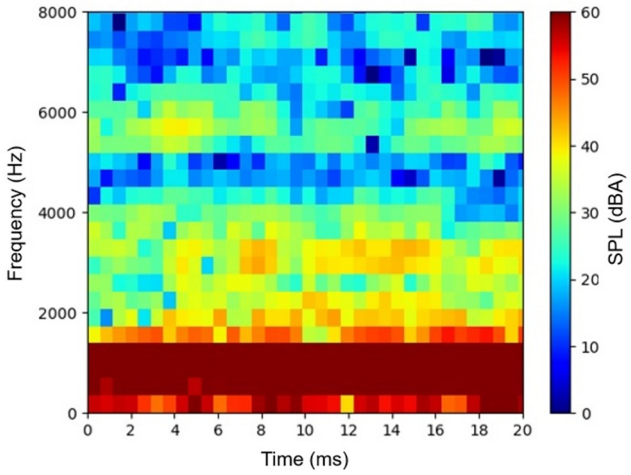

Figure 13. Spectrum for the motor with a short-circuit fault.

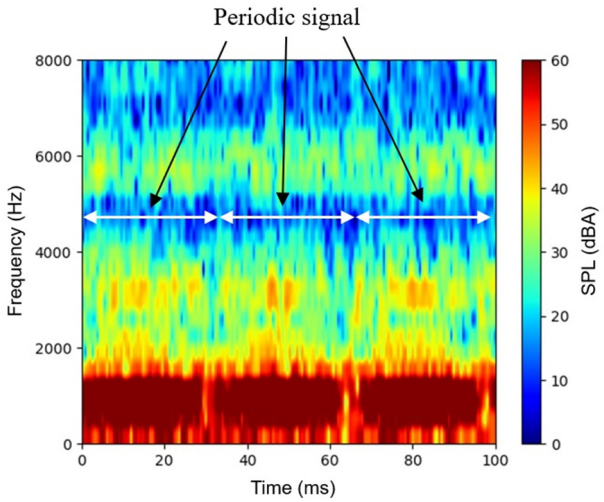

Figure 14. Spectrum for the motor with a short-circuit fault.

4. Methodology for Diagnosis

4.1. Long Short-Term Memory (LSTM) [27]

It was important to select a suitable methodology for the diagnosis of faulted as described in the previous section. In this paper, we used the generic LSTM method, which was effective for treating the sound signal.

The background and construction of LSTM are briefly explained. First, a recurrent neural network (RNN) was proposed to model the time-series data, such as speech data and music. RNN was a class of artificial neural networks. To manage the signal, RNN had a network structure in which the value of the hidden layer was inputted to the hidden layer again. However, RNN had a disadvantage because it was challenging to learn long-term time-series data because of the vanishing gradient problem. To overcome this drawback, Hochreiter and Schmidhuber [27] proposed LSTM. Since LSTM was a powerful model and could learn longer-term time-series data than RNN, it was obtaining good resulted in language processing.

Figure 15 shows the structure, and these data series control methods are expressed Equations (1)–(6):

$$f_t = \sigma(W_f[h_{t-1}, x_t] + b_f) \tag{1}$$

$$i_t = \sigma(W_i[h_{t-1}, x_t] + b_i) \tag{2}$$

$$o_t = \sigma(W_o[h_{t-1}, x_t] + b_o) \tag{3}$$

$$\hat{c_t} = tanh(W_c[h_{t-1}, x_t] + b_c) \tag{4}$$

$$c_t = f_t \times c_{t-1} + i_t \times \hat{c_t} \tag{5}$$

$$h_t = o_t \times \tan \mathrm{h}(c_t) \tag{6}$$

where $x(t)$ is the current input, W_f, W_i, W_c and W_o are weights, b_f, b_i, b_c and b_o are biases, respectively. $\sigma(x)$ is the sigmoid function, f_t, i_t, o_t are the forget gate, input gate and output gate, respectively.

LSTM is more stable than the classical RNN and can theoretically retain information for prolonged periods.

4.2. Training of LSTM

In order to use LSTM, we needed to decide the structure of the LSTM network. In constructing LSTM, we applied the free software Python, which is the most popular programming language in the world and is widely used in data science and for producing deep learning algorithms.

First, the number of input units was decided. Since 128 points were used in STFT in Section 3, 64 order frequency components were obtained. Moreover, by adding one bios term to them, the number of input units was set to be 65.

Next, the number of hidden units needed to be decided. To decide the number, both loss and accuracy were calculated while changing the number of hidden units. In this calculation, 100 data for each 5-fault condition and 200 data for health conditions were used, and the total number of data for training amounts to 700. The number of epochs was 30. Table 1 shows the final values of loss and accuracy after constructing the network. Consequently, these values depend on the difference of the hidden units. Considering the stability and reliability of the network, the number of hidden units in the network was selected as 300. Figures 16 and 17 show the relationship between epoch and both the loss and accuracy, respectively. With a diagnosis process, it is necessary to minimize the error. The objective function is often referred to as a loss function and the value of the loss function is called loss. If the prediction of the model is perfect, the loss is zero. Otherwise, the loss is greater. The discriminative ability of a diagnostic procedure is called accuracy. Accuracy is defined here by the ratio of number of data trained correctly to total number of data trained. We can find that both values were converging, and the accuracy of the network was increasing as the training proceeds.

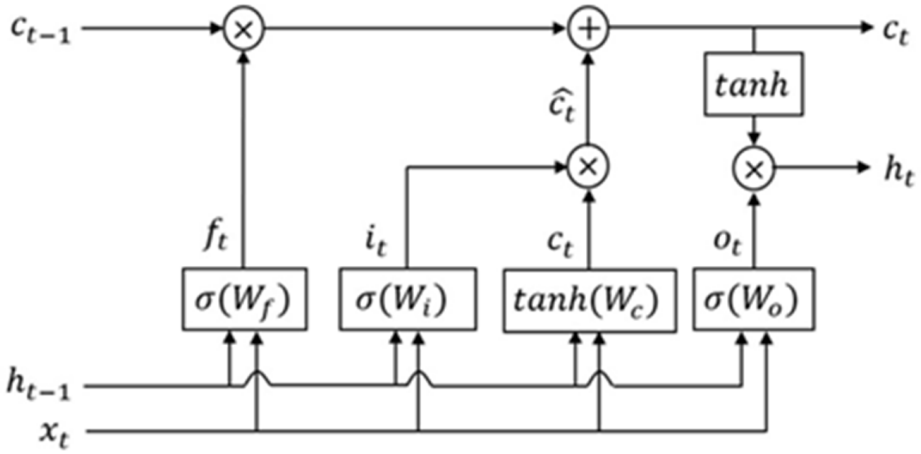

Figure 15. Structure of long short-term memory (LSTM).

Table 1. Comparison of networks.

Hidden Units	Loss	Accuracy (%)
100	0.106	97.8
200	0.077	97.9
300	0.017	99.7
400	0.018	99.6
500	0.013	99.7

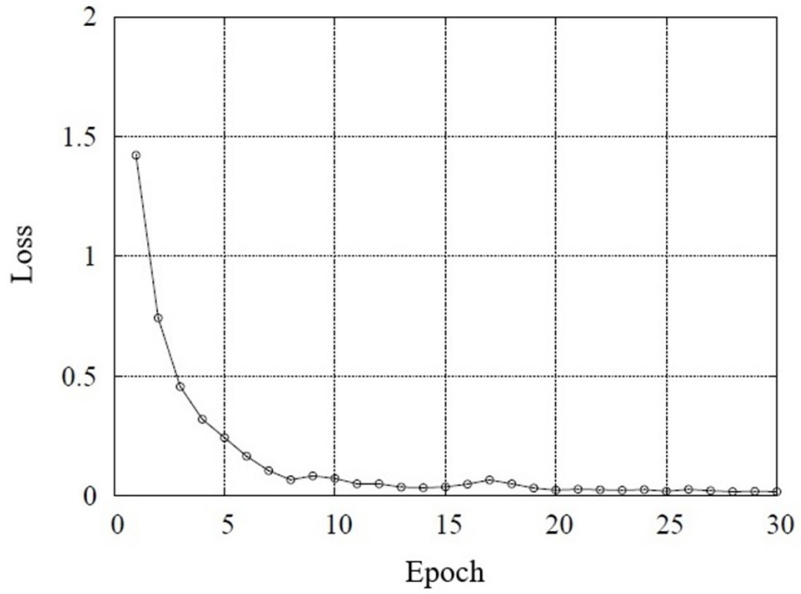

Figure 16. Relationship between the number of epoch and the value of loss.

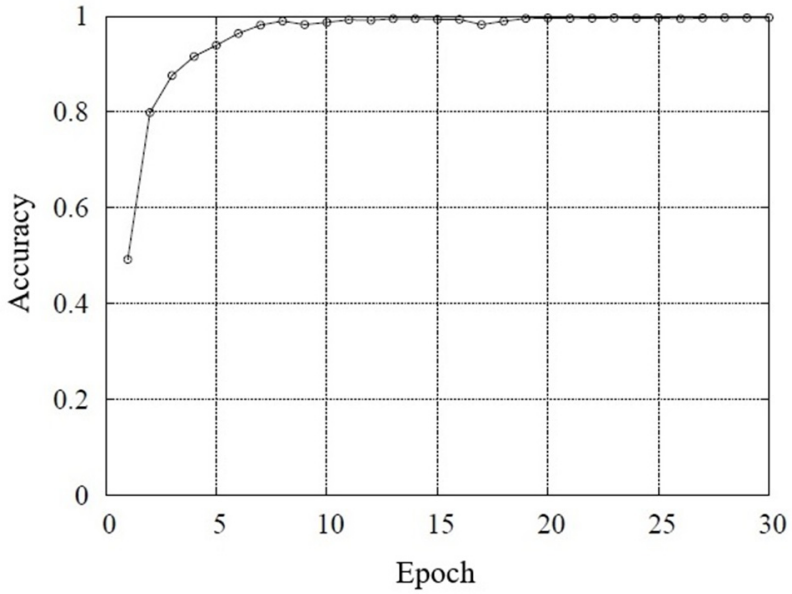

Figure 17. Relationship between the number of epoch and the value of accuracy.

5. Evaluation

5.1. Evaluation of Accuracy

In the training phase of the network, 100 rotating sound data obtained from two healthy motors and 30 rotating sound data obtained from each motor with faults were used. In the evaluation phase, without using data that are used in the training phase, 90 rotating sound data obtained from three new motors and 30 rotating sound data obtained from each faulty motor are used.

Table 2 shows the diagnostic results. For easy understanding, the following description is used in this table. "He" is a healthy motor, "1H05" is one hole with a diameter of 0.5 mm in the bearing, "1H20" is one hole with a diameter of 2.0 mm in the bearing, "2H20" is two holes with diameters of 2.0 mm in the bearing, "Sc" is a fault motor with a scratch in the bearing, and "Sh" is a fault motor with a short-circuit fault in the stator winding. From Table 2, the accuracy of the diagnosis was 100%, even for the slight fault; 1H05, Sr and Sh. Moreover, the different types of fault were identified obviously. It proves that the proposed method is effective for practical use.

Next, we evaluate the relationship between the accuracy of diagnosis and the shift time of STFT, which were calculated by shifting them by 1.2 ms and 2.0 ms, respectively. When the shift time is 1.2 ms, the accuracy for each condition remained 100%.

Table 3 shows the accuracy when the shift time is 2.0 ms. Here, some sound data obtained under healthy conditions were mistaken for the one hole with a diameter of 0.5 mm, and the number of times of misrecognition increased. Figures 18 and 19 show the STFT results. Many similar parts exist in these figures, and it is challenging to find the periodic signals appearing in the spectra, as shown in Section 3. It is considered that the accuracy of the diagnosis decreased because of the usage of the spectrum with a lower resolution to the LSTM. Nevertheless, the diagnostic accuracy of 85.6% is achieved, and the value is practically acceptable. This is because the average of sound spectra obtained in a few seconds is used for diagnosis instead of only one sound spectrum. The results suggest that usage of the average sound spectrum is important to obtain high accuracy for some shift times in STFT.

Table 2. Results of diagnosis.

	Motor Condition	Target Motor					
		He	**1H05**	**1H20**	**2H20**	**Sc**	**Sh**
Results of diagnosis	He	90	0	0	0	0	0
	1H05	0	30	0	0	0	0
	1H20	0	0	30	0	0	0
	2H20	0	0	0	30	0	0
	Sc	0	0	0	0	30	0
	Sh	0	0	0	0	0	30
Accuracy average (%)		100	100	100	100	100	100

Table 3. Results of diagnosis (shift time: 2.0 ms).

	Motor Condition	Target Motor					
		He	**1H05**	**1H20**	**2H20**	**Sc**	**Sh**
Results of diagnosis	He	77	0	0	0	0	0
	1H05	13	30	0	0	0	0
	1H20	0	0	30	0	0	0
	2H20	0	0	0	30	0	0
	Sc	0	0	0	0	30	0
	Sh	0	0	0	0	0	30
Accuracy average (%)		85.6	100	100	100	100	100

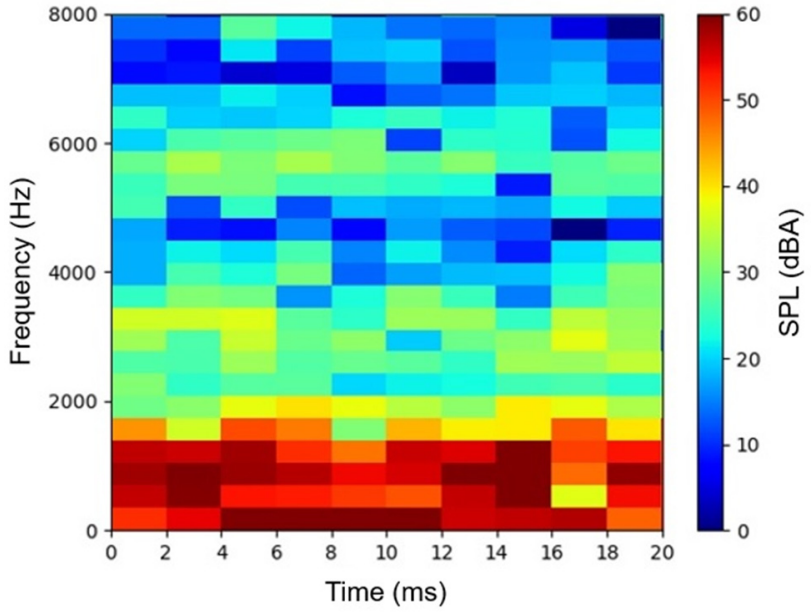

Figure 18. Spectrum for the healthy motor (shift time: 2.0 ms).

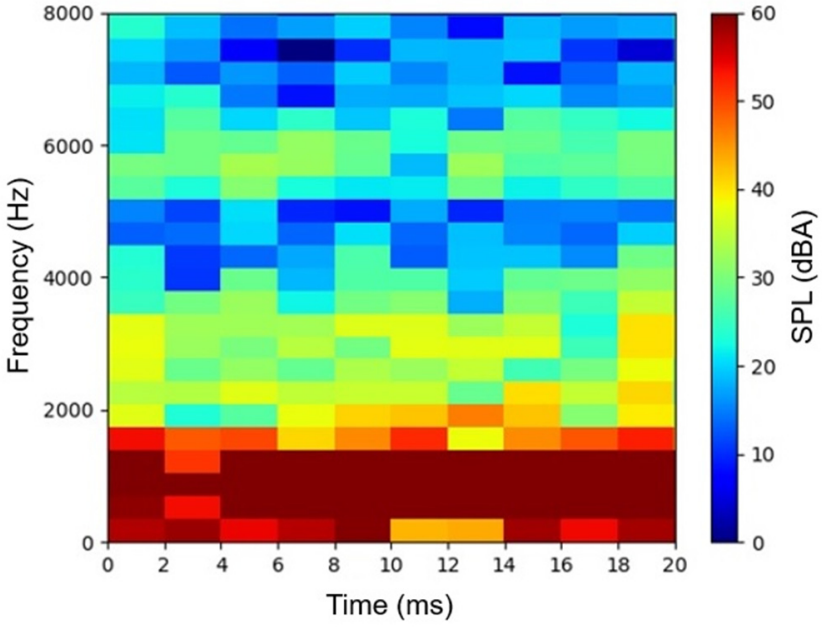

Figure 19. Spectrum for the motor with 1 hole with a diameter of 0.5 mm (shift time: 2.0 ms).

5.2. Discussion

In order to evaluate the effectiveness of the proposed method, two additional new healthy motors and one motor with one hole with a diameter of 0.5 mm were prepared. The rotating sounds were measured and evaluated. For easy understanding, two healthy motors and a motor with one hole with a diameter of 0.5 mm are named "He-A1", "He-A2" and "1H05-A1", respectively. In this evaluation, 30 rotating sound data obtained from each motor were used.

Table 4 shows the diagnostic results. Thirty data for "He-A1" and "1H05-A1" were correctly identified as "He" and "1H05", respectively. The accuracies of the diagnosis were 100%. On the other hand, the accuracy of the diagnosis for "He-A2" decreased to 90.0%. Though some misrecognition occurs, and the total accuracy of the diagnosis decreases, it is still high, and the proposed method is considered effective for practical use.

Table 4. Results of diagnosis for additional motors.

	Motor Condition	**Target Motor**		
		He-A1	**He-A2**	**1H05-A1**
Results of diagnosis	He	30	27	0
	1H05	0	3	30
	1H20	0	0	0
	2H20	0	0	0
	Sc	0	0	0
	Sh	0	0	0
Accuracy average (%)		100	90.0	100

6. Conclusions

This study presented a strategy for diagnosing minor bearing and short-circuit faults in the stator winding using the rotating sound of the motor measured at no-load condition. First, several motors were prepared, and the rotating sounds were measured. Second, the rotating sounds were analyzed, and we revealed that the characteristic signal was included in both of frequency and time domain. Taking into account the characteristics, a diagnosis

method based on deep learning was prepared. Finally, the effectiveness of the method was performed by experiments, and excellent performance was achieved.

The proposed method has the following advantages.

- The diagnosis system is simple and can be realized at a low-cost. A microphone is cheap, and the free software Python is available for programming based on deep learning;
- Extremely high accuracy rate of diagnosis is achieved for at least conditions described in the present paper;
- A fault motor can be discriminated from a healthy motor. It can detect a slight fault in bearing or stator winding like a hole of 0.5 mm diameter on an outer raceway of a bearing, one turn-to-turn short circuit of the stator winding;
- Furthermore, a kind of fault can be identified;
- A possible application of the proposed method is a shipping test of motors at manufactures. Reduction in labor, cost, and time of the test can be expected.

On the other hand, there are still several issues to be considered. Optimization of the installation location of a microphone, evaluation of the proposed system by applying load on a motor will be carried out in the future study.

Author Contributions: Conceptualization, H.N.; methodology, H.N.; validation, K.A. and S.U.; formal analysis, K.A. and S.U.; investigation, H.N. and Y.M.; resources, H.N. and Y.M.; data curation, K.A. and S.U.; writing—original draft preparation, H.N.; writing—review and editing, H.N. and Y.M.; visualization, H.N.; supervision, H.N.; project administration, H.N.; funding acquisition, H.N. and Y.M. All authors have read and agreed to the published version of the manuscript.

Funding: This research received no external funding.

Conflicts of Interest: The authors declare no conflict of interest.

References

1. Motor Reliability Working Group. Report of Large Motor Reliability Survey of Industrial and Commercial Installation, Part II. *IEEE Trans. Ind. Appl.* **1985**, *21*, 865–872.
2. Zhou, W.; Lu, B.; Habetler, T.G.; Harley, R.G. Incipient Bearing Fault Detection via Motor Stator Current Noise Cancellation Using Wiener Filter. *IEEE Trans. Ind. Appl.* **2009**, *45*, 1309–1317. [CrossRef]
3. Delgado, M.; Cirrincione, G.; Garcia, A.; Ortega, J.A.; Henao, H. A novel condition monitoring scheme for bearing faults based on curvilinear component analysis and hierarchical neural networks. In Proceedings of the 2012 XXth International Conference on Electrical Machines, Marseille, France, 2–5 September 2012; pp. 2472–2478.
4. Prieto, M.D.; Cirrincione, G.; Espinosa, A.G.; Qrtega, J.A.; Henao, H. Bearing fault diagnosis by a novel condition-monitoring scheme based on statistical-time features and neural networks. *IEEE Trans. Ind. Electron.* **2013**, *60*, 3398–3407. [CrossRef]
5. Jin, X.; Zhao, M.; Chow, T.W.S.; Pecht, M. Motor Bearing Fault Diagnosis Using Trace Ratio Linear Discriminant Analysis. *IEEE Trans. Ind. Electron.* **2014**, *61*, 2441–2451. [CrossRef]
6. Seshadrinath, J.; Singh, B.; Panigrahi, B.K. Investigation of Vibration Signatures for Multiple Fault Diagnosis in Variable Frequency Drives Using Complex Wavelets. *IEEE Trans. Power Electron.* **2014**, *29*, 936–945. [CrossRef]
7. Wang, J.; Peng, Y.; Qiao, W.; Hudgins, J.L. Bearing fault diagnosis of Direct-Drive Wind Turbines Using Multiscale Filtering Spectrum. *IEEE Trans. Ind. Appl.* **2017**, *53*, 3029–3038. [CrossRef]
8. Saucedo-Dorantes, J.J.; Delgado-Prieto, M.; Osornio-Rios, R.A.; Romero-Troncoso, R.D.J. Multifault Diagnosis Method Applied to an Electric Machine Based on High-Dimensional Feature Reduction. *IEEE Trans. Ind. Appl.* **2016**, *53*, 3086–3097. [CrossRef]
9. Ewert, P.; Orlowska-Kowalska, T.; Jankowska, K. Effectiveness Analysis of PMSM Motor Rolling Bearing Fault Detections Based on Vibration Analysis and Shallow Neural Networks. *Energies* **2021**, *14*, 712. [CrossRef]
10. Lau, E.C.C.; Ngan, H.W. Detection of motor bearing outer raceway detect by wavelet packet transformed motor current signature analysis. *IEEE Trans. Instrum. Meas.* **2010**, *59*, 2683–2690. [CrossRef]
11. Frosini, L.; Bassi, E. Stator Current and Motor Efficiency as Indicators for Different Types of Bearing Faults in Induction Motors. *IEEE Trans. Ind. Electron.* **2010**, *57*, 244–251. [CrossRef]
12. Leite, V.C.M.N.; Silva, J.G.B.; Veloso, G.F.C.; Silva, L.E.D.; Lambert-Torres, G.; Bonaldi, E.L.; Oliveria, L.E.L. Detection of Localized Bearing Faults in Induction Machines by Spectral Kurtosis and Envelope Analysis of Stator Current. *IEEE Trans. Indu. Electron.* **2015**, *62*, 1855–1865. [CrossRef]
13. Boudinar, A.H.; Benouzaa, N.; Bendiabdellah, A.; Khodja, M.E.A. Induction Motor Bearing Fault Analysis Using a Root-MUSIC Method. *IEEE Trans. Ind. Appl.* **2016**, *52*, 3851–3860. [CrossRef]

14. Pandarakone, S.E.; Mizuno, Y.; Nakamura, H. Distinct Fault Analysis of Induction Motor Bearing Using Frequency Spectrum Determination and Support Vector Machine. *IEEE Trans. Ind. Appl.* **2016**, *53*, 3049–3056. [CrossRef]
15. Pandarakone, S.E.; Mizuno, Y.; Nakamura, H. Evaluating the Progression and Orientation of Scratches on Outer-Raceway Bearing Using a Pattern Recognition Method. *IEEE Trans. Ind. Electron.* **2018**, *66*, 1307–1314. [CrossRef]
16. Kang, M.; Kim, J.; Wills, L.; Kim, J.M. Time-Varying and Multiresolution Envelope Analysis and Discriminative Feature Analysis for Bearing Fault Diagnosis. *IEEE Trans. Ind. Electron.* **2015**, *62*, 7749–7761. [CrossRef]
17. Hamadache, M.; Lee, D.; Veluvolu, K.C. Rotor Speed-Based Bearing Fault Diagnosis (RSB-BFD) Under Variable Speed and Constant Load. *IEEE Trans. Ind. Electron.* **2015**, *62*, 6486–6495. [CrossRef]
18. Geiman, J. DC Step-Voltage and Surge Testing Motors. Available online: https://www.efficientplantmag.com/2007/03/dc-step-voltage-and-surge-testing-of-motors/ (accessed on 13 January 2021).
19. Yang, S.C. Online Stator Turn Fault Detection for Inverter-Fed Electric Machines Using Neutral Point Voltages Difference. *IEEE Trans. Ind. Appl.* **2016**, *52*, 4039–4049. [CrossRef]
20. Bouzid, M.B.K.; Champenois, G. An Efficient Simplified Physical Faulty Model of a Permanent Magnet Synchronous Generator Dedicated to Stator Fault Diagnosis Part II: Automatic Stator Fault Diagnosis. *IEEE Trans. Ind. Appl.* **2017**, *53*, 2762–2771. [CrossRef]
21. Pandarakone, S.E.; Mizuno, Y.; Nakamura, H. Online Slight Inter-Turn Short-Circuit Fault Diagnosis Using the Distortion Ratio of Load Current in a Low-Voltage Induction Motor. *IEEJ J. Ind. Appl.* **2018**, *7*, 473–478. [CrossRef]
22. Saleh, S.A.; Ozkop, E. Phaselet-Based Method for Detecting Electric Faults in 3ϕ Induction Motor Drives—Part I: Analysis and Development. *IEEE Trans. Ind. Appl.* **2017**, *53*, 2976–2987. [CrossRef]
23. Irhoumah, M.; Pusca, R.; Lefevre, E.; Mercier, D.; Romary, R. Detection of the Stator Winding Inter-Turn Faults in Asynchronous and Synchronous Machines Through the Correlation Between Harmonics of the Voltage of Two Magnetic Flux Sensors. *IEEE Trans. Ind. Appl.* **2019**, *55*, 2682–2689. [CrossRef]
24. Gyftakis, K.N.; Sumislawska, M.; Kavanagh, D.F.; Howey, D.A.; McCulloch, M.D. Dielectric Characteristics of Electric Vehicle Traction Motor Winding Insulation Under Thermal Aging. *IEEE Trans. Ind. Appl.* **2016**, *52*, 1398–1404.
25. Sumislawska, M.; Gyftakis, K.N.; Kavanagh, D.F.; McCulloch, M.D.; Burnham, K.J.; Howey, D.A. The Impact of Thermal Degradation on Properties of Electrical Machine Winding Insulation Material. *IEEE Trans. Ind. Appl.* **2016**, *52*, 2951–2960. [CrossRef]
26. Mizusawa, T.; Kondo, Y.; Takizawa, N.; Kawaharada, Y. Fundamental Study on Impact Sound Generated from Plates Colliding Spherical Bodies. *Proc. Jpn. Soc. Civil Eng.* **2004**, *766*, 47–57. (In Japanese)
27. Hochreiter, S.; Schmidhuber, J. Long Short-Term Memory. *Neural Comput.* **1997**, *9*, 1735–1780. [CrossRef]